Upscaling matrix diffusion coefficients for heterogeneous fractured rocks

Zhenxue Dai,[1] Andrew Wolfsberg,[1] Zhiming Lu,[1] and Paul Reimus[1]

Received 12 January 2007; revised 5 March 2007; accepted 13 March 2007; published 14 April 2007.

[1] The scale dependence of the matrix diffusion coefficient (D_m) for fractured media has been observed at variable scales from column experiments to field tracer tests. In this paper, we derive an effective D_m for multimodal heterogeneous fractured rocks using characteristic distributions of matrix properties and volume averaging of the mass transfer coefficient. The effective field-scale D_m is dependent on the statistics (geometric mean, variance, and integral scale) of laboratory-scale $\ln(D_m)$ and on the domain size. The effective D_m increases with the integral scales and is larger than the geometric mean of $\ln(D_m)$. Monte Carlo simulations with 1000 realizations of heterogeneous D_m fields were conducted to assess the accuracy of the derived effective D_m.
Citation: Dai, Z., A. Wolfsberg, Z. Lu, and P. Reimus (2007), Upscaling matrix diffusion coefficients for heterogeneous fractured rocks, *Geophys. Res. Lett.*, *34*, L07408, doi:10.1029/2007GL029332.

1. Introduction

[2] In saturated fractured-rock systems, where the primary pathway for groundwater flow and solute transport is through fractures, groundwater in the matrix is considered immobile in dual-porosity conceptual models [*Tang et al.*, 1981; *Sudicky and Frind*, 1982]. Thus, although the bulk of the water travels through the fractures, a very large reservoir of water in the matrix can act to store and reduce mobility of contaminants via matrix diffusion [*Robinson*, 1994]. *Carrera et al.* [1998] presented a comprehensive study of matrix diffusion and concluded that D_m is one of the parameters that govern contaminant transport in fractured rocks. Recent field-scale tracer test interpretations by *Reimus and Callahan* [2007] highlighted the significance of fracture apertures in governing mass transfer between fractures and matrix, particularly when the field-scale fractures in which solutes flow may have larger apertures than those used in laboratory columns. Ultimately, mass transfer between fractures and matrix depends on D_m, fracture aperture, and matrix porosity. This paper addresses scaling of heterogeneous D_m.

[3] Over the years, the ability to fully characterize the parameters in the fracture-matrix mass transfer process has not kept pace with numerical and modeling expertise [*Liu et al.*, 2007]. Transport experiments are usually conducted at the sub-meter or column scale under conditions in which flow rates, tracer injections and other conditions are well controlled. Assuming relatively little heterogeneity in such experiments, analytical or semi-analytical models have been used to estimate fracture transport parameters [*Cormenzana*, 2000]. However, there remains no practical unifying theory to integrate laboratory-scale parameters in field-scale predictions for risk assessment or remedial design.

[4] Recent studies indicate that D_m estimated from the column transport experiments may not be suitable for modeling field-scale solute transport in fractured rocks. *Shapiro* [2001] reported that effective D_m in kilometer-scale systems is much greater than estimates from laboratory experiments due to complex, possibly advective, field-scale transport processes. *Neretnieks* [2002] and *Andersson et al.* [2004] estimated the effective D_m from field tracer test data at the Äspö site and obtained some values about 30 times greater than their laboratory-scale estimates, which they attributed to increased diffusion surface area in their field test. *Liu et al.* [2004] reported that the effective D_m at the field scale is generally greater than that at laboratory scales and tends to increase with the testing scale. While several potential mechanisms have been identified, they found that this interesting scale dependence may be related to rock matrix heterogeneity in fractured rock. Based on numerical experiments, *Zhang et al.* [2006] empirically determined a formula for estimating the effective D_m. However, their equation does not show dependence of the effective D_m on the spatial scales.

[5] The work we present here focuses on the spatial-scale dependence of the effective D_m in multimodal heterogeneous rocks. We start from characterization of heterogeneous matrix properties to build the covariance function of $\ln(D_m)$. Then, we derive equations to describe the relationship between the effective D_m, the statistics of D_m measurements at laboratory scales, and the domain size. Monte Carlo simulations are performed to assess the accuracy of the derived effective D_m in a synthetic example.

2. Spatial Statistics of Multimodal D_m

[6] Spatial covariance models developed from centimeter-scale measurements are important in upscaling effective parameters at larger scales. To characterize heterogeneous aquifer system, *Lu and Zhang* [2002] and *Ritzi et al.* [2004] presented a general form of multimodal correlation model of permeability. Here we apply it to modeling the covariance of $\ln(D_m)$. Heterogeneity of D_m comes from the variations of matrix physical and chemical properties within and across matrix units. Assuming a field-scale model made up of N matrix units in mutually exclusive occurrences (see Figure 1, $N = 3$), the distribution of matrix properties can be characterized by an indicator random variable $I_k(\boldsymbol{x})$,

$$I_k(\boldsymbol{x}) = \begin{cases} 1, \text{if unit } k \text{ occurs at location } \boldsymbol{x} \\ 0, \text{otherwise.} \end{cases} \quad (1)$$

[1]Hydrology and Geochemistry Group, Earth and Environmental Sciences Division, Los Alamos National Laboratory, Los Alamos, New Mexico, USA.

0094-8276/07/2007GL029332$05.00

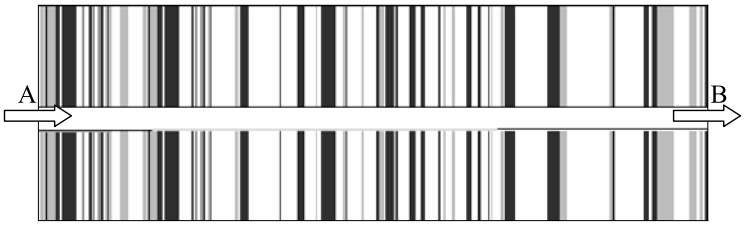

Figure 1. Heterogeneous matrix with three units created with TPROG [*Carle and Fogg*, 1997] by using the data listed in Table 1 (U1 = white, U2 = grey, and U3 = black). The fracture half aperture is 0.01 m and the fracture spacing is 2 m.

Then, the $\ln(D_m)$, denoted as $Y(\boldsymbol{x})$, can be expressed as

$$Y(\boldsymbol{x}) = \sum_{k=1}^{N} I_k(\boldsymbol{x}) Y_k(\boldsymbol{x}), \tag{2}$$

where $Y_k(\boldsymbol{x})$ represents $\ln(D_m)$ within unit k. If the volume fraction of unit k is denoted as p_k, the expected value of I_k is equal to p_k ($k = 1, 2, \ldots, N$). The composite mean M_Y and variance σ_Y^2 of $Y(\boldsymbol{x})$ can be expressed as [see *Ritzi et al.*, 2004]

$$M_Y = \sum_{k=1}^{N} p_k m_k, \quad \sigma_Y^2 = \sum_{k=1}^{N} p_k \sigma_k^2 + \frac{1}{2} \sum_{k=1}^{N} \sum_{i=1}^{N} p_k p_i (m_k - m_i)^2, \tag{3}$$

where m_k and σ_k^2 denote the mean and variance of $Y_k(\boldsymbol{x})$, respectively.

[7] Using indicator variables, we apply the transition probability for measuring spatial continuity of facies distributions [*Carle and Fogg*, 1997]. The transition probability in φ direction, $t_{ki}(\boldsymbol{h}_\varphi)$, is defined by

$$t_{ki}(\boldsymbol{h}_\varphi) = \Pr\{I_i(\boldsymbol{x} + \boldsymbol{h}_\varphi) = 1 \text{ and } I_k(\boldsymbol{x}) = 1\} / \Pr\{I_k(\boldsymbol{x}) = 1\}, \tag{4}$$

where $\boldsymbol{h}_\varphi$ is the lag distance in φ direction. Similar to the permeability covariance defined by *Dai et al.* [2005], the composite covariance $C_Y(\boldsymbol{h}_\varphi)$ of $Y(\boldsymbol{x})$ can be represented in the term of proportion, transition probability, and the in-unit or cross-unit covariance of $Y_k(\boldsymbol{x})$ as

$$C_Y(\boldsymbol{h}_\varphi) = \sum_{k=1}^{N} \sum_{i=1}^{N} \{C_{ki}(\boldsymbol{h}_\varphi) + m_k m_i\} p_k t_{ki}(\boldsymbol{h}_\varphi) - M_y^2. \tag{5}$$

By assuming that the cross-covariances are negligible, i.e., $C_{ki}(\boldsymbol{h}_\varphi) = 0$ for $k \neq i$ [*Dai et al.*, 2004], we can write the covariance of multimodal $Y(\boldsymbol{x})$ in the following form:

$$C_Y(\boldsymbol{h}_\varphi) = \sum_{k=1}^{N} p_k C_{kk}(\boldsymbol{h}_\varphi) t_{kk}(\boldsymbol{h}_\varphi) + \frac{1}{2} \sum_{k=1}^{N} \sum_{i=1}^{N} (m_k - m_i)^2 p_k \cdot (p_i - t_{ki}(\boldsymbol{h}_\varphi)). \tag{6}$$

As derived by *Dai et al.* [2004], we use exponential functions for transition probability and auto-covariance $C_{kk}(\boldsymbol{h}_\varphi)$,

$$t_{ki}(\boldsymbol{h}_\varphi) = p_i + (\delta_{ki} - p_i) e^{-\boldsymbol{h}_\varphi / \lambda_I} \qquad (k, i = \overline{1, N}), \tag{7}$$

$$C_{kk}(\boldsymbol{h}_\varphi) = \sigma_k^2 e^{-\boldsymbol{h}_\varphi / \lambda_k} \qquad (k = \overline{1, N}), \tag{8}$$

where δ_{ki} is the Kronecker delta, λ_I is the correlation length of the indicator variable in φ direction, and λ_k is the integral scale of $Y_k(\boldsymbol{x})$, which is a measure of spatial correlation of $Y_k(\boldsymbol{x})$, roughly the distance beyond which an attribute is considered to be uncorrelated. Substituting equations (7) and (8) into equation (6), we obtain the composite covariance function as

$$C_Y(\boldsymbol{h}_\varphi) = \sum_{k=1}^{N} p_k^2 \sigma_k^2 e^{-\frac{\boldsymbol{h}_\varphi}{\lambda_k}} + \sum_{k=1}^{N} p_k (1 - p_k) \sigma_k^2 e^{-\frac{\boldsymbol{h}_\varphi}{\lambda_\psi}} + \frac{1}{2} \sum_{k=1}^{N} \sum_{i=1}^{N} (m_k - m_i)^2 p_k p_i e^{-\frac{\boldsymbol{h}_\varphi}{\lambda_I}}, \tag{9}$$

where $\lambda_\psi = \lambda_k \lambda_I / (\lambda_k + \lambda_I)$. This covariance function will be used to upscale the D_m from the laboratory scale to the field scale.

3. Effective D_m of Multimodal Matrix

[8] *Tang et al.* [1981] utilized analytical or semi-analytical solutions to model solute transport in fractured rocks, and derived an equation to represent the mass transfer coefficient as expressed in equation (10), which describes the rate at which a particular solute transfers between fractures and the rock matrix material [similarly used by *Reimus and Callahan*, 2007]. For heterogeneous matrix material, the effective mass transfer coefficient (C_{MT}) at the field scale can be computed based on effective diffusion coefficient ($\tilde{D}_m$), effective matrix porosity ($\tilde{\phi}$) and effective fracture aperture ($\tilde{b}$) as:

$$C_{MT} = \frac{\tilde{\phi} \sqrt{\tilde{D}_m}}{\tilde{b}}. \tag{10}$$

[9] Taking the small-scale mass transfer coefficient as a spatial random variable, the effective field-scale mass transfer coefficient can be expressed as the volume averaging of small-scale mass transfer coefficients. We assume that $Y(x)$ is a one-dimensional (along flow direction), second-order stationary spatial random variable. By substituting the

small-scale porosity and the half aperture with their effective values $\tilde{\phi}$ and $\tilde{b}$, we have

$$C_{MT} = \frac{\tilde{\phi}}{\tilde{b}L}\int_L e^{\frac{1}{2}Y(x)}dx, \tag{11}$$

where L is the length of the one-dimensional domain and x is the spatial coordinate. By comparing equations (11) and (10), we obtain

$$\tilde{D}_m = \left(\frac{1}{L}\int_L e^{\frac{1}{2}Y(x)}dx\right)^2, \tag{12}$$

which focuses this evaluation on D_m variability with the assumption that $\tilde{b}$ and $\tilde{\phi}$ have been estimated. Decomposing $Y(x)$ as the mean M_Y and zero-mean perturbation $Y'(x)$, $Y(x) = M_Y + Y'(x)$, we rewrite equation (12) as a double integral in the one-dimensional domain,

$$\tilde{D}_m = \frac{1}{L^2}D_m^G\left(\int_L\int_L e^{\frac{1}{2}(Y'(x)+Y'(y))}dxdy\right), \tag{13}$$

where $D_m^G = e^{M_Y}$ is the geometric mean of laboratory-scale D_m and y is also a one-dimensional spatial variable. By using Taylor expansion and assuming the variance of $Y(x)$ smaller than unity, equation (13) becomes,

$$\tilde{D}_m = \frac{1}{L^2}D_m^G\left(\int_L\int_L\left(1+\frac{1}{2}(Y'(x)+Y'(y)) + \frac{1}{8}\left(Y'(x)^2+Y'(y)^2+2Y'(x)Y'(y)\right)\right)dxdy\right). \tag{14}$$

If we take the expectation of equation (14) to quantify the effective D_m, then

$$\langle\tilde{D}_m\rangle = D_m^G\left(1+\frac{\sigma_Y^2}{4}+\frac{1}{4L^2}\left(\int_L\int_L C_Y(x,y)dxdy\right)\right), \tag{15}$$

where, $C_Y(x,y) = \langle Y'(x)Y'(y)\rangle$ is the covariance that can be substituted using equation (9) with $h_\varphi = |x - y|$, so that φ is in the same direction as that of the one-dimensional variable. Then, we have the effective D_m as

$$\langle\tilde{D}_m\rangle = D_m^G\left(1+\frac{\sigma_Y^2}{4}+\frac{1}{2L^2}\left(\sum_{k=1}^N p_k^2\sigma_k^2\lambda_k^2\left(\frac{L}{\lambda_k}-1+e^{-\frac{L}{\lambda_k}}\right) + \sum_{k=1}^N p_k(1-p_k)\sigma_k^2\lambda_\psi^2\left(\frac{L}{\lambda_\psi}-1+e^{-\frac{L}{\lambda_\psi}}\right) + \frac{1}{2}\sum_{k=1}^N\sum_{i=1}^N (m_k-m_i)^2 p_k p_i \lambda_I^2\left(\frac{L}{\lambda_I}-1+e^{-\frac{L}{\lambda_I}}\right)\right)\right). \tag{16}$$

Table 1. Mean and Variance of $Y_k(\boldsymbol{x})$, Proportions, and Integral Scales of the Units

Units	k	p_k	m_k	D_{mk}^G, m^2/s	σ_k^2	λ_I, m	λ_k, m	λ_ψ, m
U1	1	0.64	−21.55	$4.4\cdot10^{-10}$	0.58	5	4.86	2.46
U2	2	0.14	−20.62	$1.1\cdot10^{-9}$	0.45	5	3.58	2.09
U3	3	0.22	−20.26	$1.5\cdot10^{-9}$	0.65	5	4.27	2.30

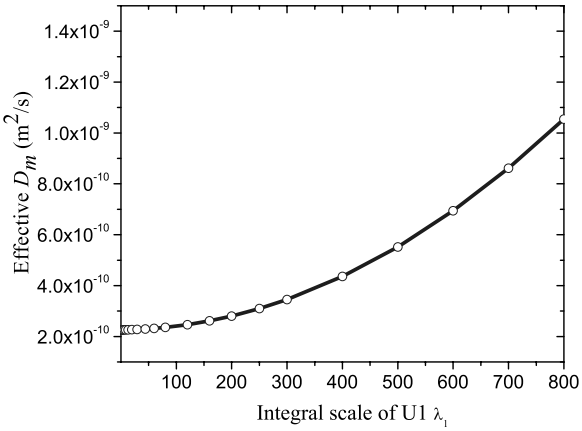

Figure 2. Effective D_m versus integral scale of U1.

[10] In equation (16), the effective D_m increases with the variance. If the matrix is homogeneous, the variance is 0 and the effective D_m is equal to the geometric mean, which indicates that the heterogeneity of matrix properties is the source of the scale dependence of D_m.

[11] To further investigate the scale dependence of D_m, we set up a synthetic field-scale heterogeneous matrix system with three units (Table 1 and Figure 1). Using equation (16) and the data listed in Table 1, we plot the effective D_m vs. the integral scale of unit 1 (U1) in Figure 2, which shows that the effective D_m increases with the increasing integral scales. Additional numerical experiments also show that the effective D_m is positively correlated to the integral scales of units 2 and 3, and the indicator correlation length.

4. Effective D_m of Bimodal and Unimodal Matrix

[12] In equation (16), if $N = 2$, $Y(\boldsymbol{x})$ follows a bimodal distribution and the expression of the effective D_m becomes,

$$\langle\tilde{D}_m\rangle = D_m^G\left(1+\frac{\sigma_Y^2}{4}+\frac{1}{2L^2}\left(\sum_{k=1}^2 p_k^2\sigma_k^2\left(\lambda_k^2\left(\frac{L}{\lambda_k}-1+e^{-\frac{L}{\lambda_k}}\right) + \lambda_\psi^2\left(\frac{L}{\lambda_\psi}-1+e^{\frac{L}{\lambda_\psi}}\right)\right) + (m_1-m_2)^2 p_1 p_2 \lambda_I^2 \cdot\left(\frac{L}{\lambda_I}-1+e^{-\frac{L}{\lambda_I}}\right)\right)\right). \tag{17}$$

If $N = 1$, $Y(\boldsymbol{x})$ follows a unimodal distribution, equation (16) can be simplified as,

$$\langle\tilde{D}_m\rangle = D_m^G\left(1+\frac{\sigma_Y^2}{4}\left(1+\frac{2\lambda^2}{L^2}\left(\frac{L}{\lambda}-1+e^{-\frac{L}{\lambda}}\right)\right)\right). \tag{18}$$

Furthermore, if $\lambda/L \to 0$, which means the field is not correlated or $Y(\boldsymbol{x})$ are totally randomly distributed, equation (18) is approximated as:

$$\langle\tilde{D}_m\rangle \approx D_m^G\left(1+\frac{\sigma_Y^2}{4}\right), \tag{19}$$

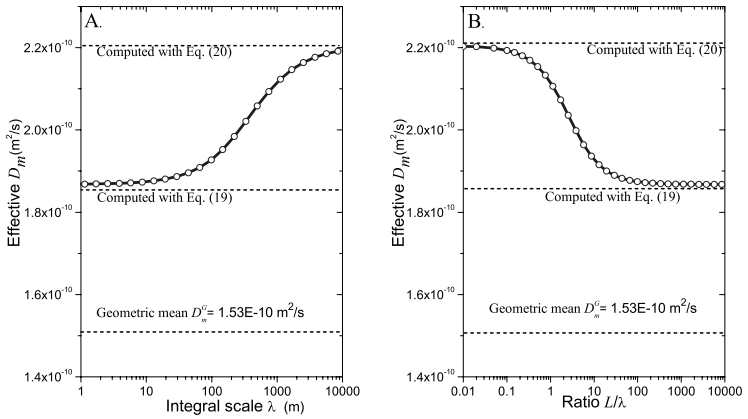

Figure 3. Effective D_m versus (a) the unimodal integral scale and (b) the ratio of domain size and integral scale.

which is a first-order approximation of *Zhang et al.* [2006, equation (10)]. On the other hand, if λ/L is sufficiently large, equation (18) is approximated as:

$$\langle \tilde{D}_m \rangle \approx D_m^G \left(1 + \frac{\sigma_Y^2}{2}\right). \tag{20}$$

[13] Assuming that in equation (18) the mean of unimodal $Y(\boldsymbol{x})$ is -22.6 ln(m^2/s), the variance is 0.88, and the domain size is 1000 m, we plot effective D_m as a function of the integral scale in Figure 3a. The effective D_m increases with the integral scale. For comparison, the effective D_m computed with equations (19) and (20), which correspond with the cases that $\lambda \to 0$ and λ is sufficiently large, are also illustrated in Figure 3a (assume L is constant). When $\lambda \to 0$, the effective D_m is $1.86 \cdot 10^{-10}$ m^2/s and is greater than the geometric mean ($1.53 \cdot 10^{-10}$ m^2/s). When λ = 300 m, it is $2.01 \cdot 10^{-10}$ m^2/s, and when λ is sufficiently large, it is $2.21 \cdot 10^{-10}$ m^2/s. Figure 3b shows that the effective D_m decreases when the ratio L/λ increases.

5. Monte Carlo Simulations

[14] To assess the accuracy of the effective D_m, we conducted Monte Carlo simulations for conservative tracer transport in unimodal fractured rocks with the generalized double porosity model (GDPM [*Zyvoloski et al.*, 2003]). The GDPM numerical model has a length of 1000 m, a fracture spacing of 2 m, and a half aperture of 0.01 m. The model has 1001 fracture nodes (constant spatial space Δx = 1 m) and 10010 matrix nodes (each fracture node connects to 10 matrix nodes perpendicular to the flow direction with variable spatial spaces from 0.01 to 0.4 m). At the first fracture node (point A in Figure 1), the water injection rate is constant at 0.0116 kg/s. In the injection water, the solute concentration is normalized to 1. For the purpose of this demonstration, the only spatial random variable in the simulations is D_m.

[15] The heterogeneous fields of unimodal $Y(x)$ were generated with a Gaussian random field generator [*Zhang and Lu*, 2004]. We generated 1000 realizations with a mean $Y(x)$ of -22.6 ln(m^2/s), variance of 0.88, and integral scale of 300 m. The quality of the generated $Y(x)$ fields was checked by comparing the covariance calculated from the generated realizations with the analytical, exponential covariance model. The comparison shows that the realizations match the specified mean, variance, and integral scale. Then, the generated $Y(x)$ are converted to D_m for GDPM models.

[16] During the Monte Carlo simulations, we compute the mean, variance, and the 95% confidence interval of the concentration breakthrough at the last fracture node (point B in Figure 1) after each simulation, and check the evolution of concentration variance and mean with the number of simulations until the solution of Monte Carlo simulations converges. Figure 4 shows that the concentration breakthrough simulated with the effective D_m computed by equation (18) matches well to the mean concentration after 1000 Monte Carlo simulations, while with the geometric mean of D_m the concentration is overestimated. This result

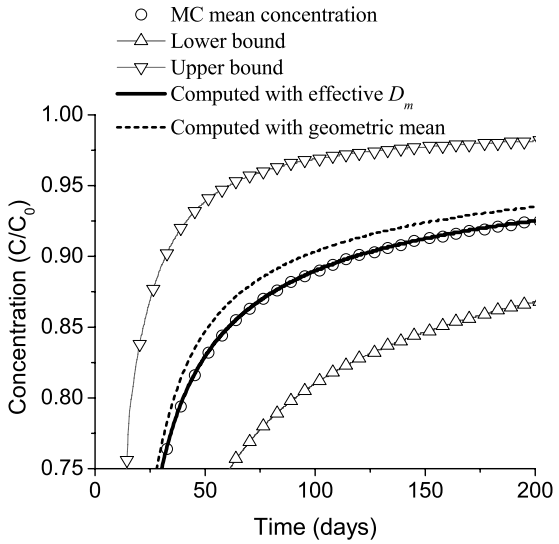

Figure 4. Computed concentration breakthroughs from the effective D_m, geometric mean and Monte Carlo simulations, as well as the concentration bounds of the 95% confidence intervals.

indicates that the derived effective D_m is an accurate estimate of D_m for the field-scale modeling.

6. Discussion and Conclusion

[17] The heterogeneity of matrix properties is the source of the scale dependence of D_m, which comes from the variations of matrix physical and chemical properties within and across matrix units. The covariance of $Y(\boldsymbol{x})$ can be used to characterize the matrix heterogeneity with transition probability of the multimodal matrix units and the covariance of $Y(\boldsymbol{x})$ within each unit. The major factors affecting D_m heterogeneity include matrix porosity, tortuosity, solute charge, and temperature. In this paper we take D_m as a lumped spatial random variable to incorporate the variation of all these factors and upscale D_m from the laboratory scale to the field scale.

[18] The effective D_m is dependent on the geometric mean, variance, integral scale, and domain size. Its value increases with the integral scale and is greater than the geometric mean. Monte Carlo simulations with 1000 realizations of heterogeneous matrix diffusion fields demonstrate that the derived effective D_m is an accurate estimation of D_m for the field-scale transport modeling in the fractured rocks. The effective D_m is derived under the condition that the variance is smaller than unity. However, the first-order perturbation might give accurate estimates of effective D_m for variance as large as 4, as discussed by *Dai et al.* [2004] for deriving macrodispersion equations. Further work is needed to identify the maximum variance that is applicable for the first-order perturbation method. The next extension of this effort will be to incorporate the influence of other processes affecting mass transfer such as spatial variations in aperture and matrix porosity.

[19] **Acknowledgments.** The reported research was supported by Los Alamos National Laboratory's Directed Research and Development Project (20070441ER). We are grateful to Bruce Robinson and Kay Birdsell for their constructive comments on the manuscript of this paper.

References

Andersson, P., J. Byegard, E. L. Tullborg, T. Doe, J. Hermanson, and A. Winberge (2004), In situ tracer tests to determine retention properties of a block scale fracture network in granitic rock at the Aspo Hard Rock Laboratory, Sweden, *J. Contam. Hydrol.*, *70*(3–4), 271–297.

Carle, S. F., and G. E. Fogg (1997), Modeling spatial variability with one- and multi-dimensional continuous Markov chains, *Math. Geol.*, *29*(7), 891–918.

Carrera, J., X. Sánchez-Vila, I. Benet, A. Medina, G. Galarza, and J. Guimerà (1998), On matrix diffusion: Formulations, solution methods, and qualitative effects, *Hydrogeol. J.*, *6*, 178–190.

Cormenzana, J. (2000), Transport of a two-member decay chain in a single fracture: Simplified analytical solution for two radionuclides with the same transport properties, *Water Resour. Res.*, *36*(5), 1339–1346.

Dai, Z., R. W. Ritzi, C. Huang, D. F. Dominic, and Y. Rubin (2004), Transport in heterogeneous sediments with multimodal conductivity and hierarchical organization across scales, *J. Hydrol.*, *294*(1–3), 68–86.

Dai, Z., R. W. Ritzi Jr., and D. F. Dominic (2005), Improving permeability semivariograms with transition probability models of hierarchical sedimentary architecture derived from outcrop analog studies, *Water Resour. Res.*, *41*, W07032, doi:10.1029/2004WR003515.

Liu, H. H., G. S. Bodvarsson, and G. Zhang (2004), Scale dependency of the effective matrix diffusion coefficient, *Vadose Zone J.*, *3*(1), 312–315.

Liu, H. H., Y. Q. Zhang, Q. Zhou, and F. J. Molz (2007), An interpretation of potential scale dependence of the effective matrix diffusion coefficient, *J. Contam. Hydrol.*, *90*(1–2), 41–57.

Lu, Z., and D. Zhang (2002), On stochastic modeling of flow in multimodal heterogeneous formations, *Water Resour. Res.*, *38*(10), 1190, doi:10.1029/2001WR001026.

Neretnieks, I. (2002), A stochastic multi-channel model for solute transport—Analysis of tracer tests in fractured rock, *J. Contam. Hydrol.*, *55*(3–4), 175–211.

Reimus, P. W., and T. J. Callahan (2007), Matrix diffusion rates in fractured volcanic rocks at the Nevada Test Site: Evidence for a dominant influence of effective fracture apertures, *Water Resour. Res.*, doi:10.1029/2006WR005746, in press.

Ritzi, R. W., Z. Dai, D. F. Dominic, and Y. Rubin (2004), Spatial correlation of permeability in cross-stratified sediment with hierarchical architecture, *Water Resour. Res.*, *40*, W03513, doi:10.1029/2003WR002420.

Robinson, B. A. (1994), A strategy for validating a conceptual model for radionuclide migration in the saturated zone beneath Yucca Mountain, *Radioact. Waste Manage. Environ. Restor.*, *19*, 73–96.

Shapiro, A. M. (2001), Effective matrix diffusion in kilometer-scale transport in fractured crystalline rock, *Water Resour. Res.*, *37*(3), 507–522.

Sudicky, E. A., and E. O. Frind (1982), Contaminant transport in fractured porous media: Analytic solutions for a system of parallel fractures, *Water Resour. Res.*, *18*(6), 1634–1642.

Tang, D. H., E. O. Frind, and E. A. Sudicky (1981), Contaminant transport in fractured porous media: Analytical solution for a single fracture, *Water Resour. Res*, *17*(3), 555–564.

Zhang, D., and Z. Lu (2004), An efficient, higher-order perturbation approach for flow in randomly heterogeneous porous media via Karhunen-Loeve decomposition, *J. Comput. Phys.*, *194*(2), 773–794.

Zhang, Y., H. Liu, Q. Zhou, and S. Finsterle (2006), Effects of diffusive property heterogeneity on effective matrix diffusion coefficient for fractured rock, *Water Resour. Res.*, *42*, W04405, doi:10.1029/2005WR004513.

Zyvoloski, G. A., B. A. Robinson, Z. V. Dash, and L. L. Trease (2003), Summary of models and methods for the FEHM Application—A finite-element heat and mass-transfer code, *Los Alamos Natl. Lab. Rep. LA-13307–MS*, Los Alamos Natl. Lab., Los Alamos, N. M.

Z. Dai, A. Wolfsberg, Z. Lu, and P. Reimus, Hydrology & Geochemistry Group, Earth and Environmental Sciences Division, Los Alamos National Laboratory, Los Alamos, NM 87545, USA. (daiz@lanl.gov)